

Research Article

Iterative PSF Estimation and Its Application to Shift Invariant and Variant Blur Reduction

Seung-Won Jung,¹ Byeong-Doo Choi,² and Sung-Jea Ko¹

¹ Department of Electronics Engineering, Korea University, Anam-Dong, Sungbuk-Ku, Seoul 136-701, South Korea

² Fraunhofer Institute for Telecommunications, Heinrich-Hertz-Institut (HHI), 10587 Berlin, Germany

Correspondence should be addressed to Sung-Jea Ko, sjko@korea.ac.kr

Received 16 February 2009; Accepted 8 October 2009

Recommended by Stephen Marshall

Among image restoration approaches, image deconvolution has been considered a powerful solution. In image deconvolution, a point spread function (PSF), which describes the blur of the image, needs to be determined. Therefore, in this paper, we propose an iterative PSF estimation algorithm which is able to estimate an accurate PSF. In real-world motion-blurred images, a simple parametric model of the PSF fails when a camera moves in an arbitrary direction with an inconsistent speed during an exposure time. Moreover, the PSF normally changes with spatial location. In order to accurately estimate the complex PSF of a real motion blurred image, we iteratively update the PSF by using a directional spreading operator. The directional spreading is applied to the PSF when it reduces the amount of the blur and the restoration artifacts. Then, to generalize the proposed technique to the linear shift variant (LSV) model, a piecewise invariant approach is adopted by the proposed image segmentation method. Experimental results show that the proposed method effectively estimates the PSF and restores the degraded images.

Copyright © 2009 Seung-Won Jung et al. This is an open access article distributed under the Creative Commons Attribution License, which permits unrestricted use, distribution, and reproduction in any medium, provided the original work is properly cited.

1. Introduction

Due to the degradation of the image caused by the limited performance of optical and electronic devices of in today's cameras, the image restoration has been researched in literature. In classical image restoration, the PSF is assumed to be known prior to the restoration process [1]. However, in real-world applications, an observed image is only available with insufficient *a priori* information.

Various techniques have been proposed to estimate the PSF. Early works on blur identification, or the estimation of the PSF, have been proposed based on regular patterns of zeros in the frequency domain [2]. However, these methods are sensitive to Gaussian blur that does not have zeros in the frequency domain. To deal with this problem, the spatial domain Bayesian parameter estimation of the PSF has been widely adopted [3, 4]. Especially in the case of motion blur, the PSF is assumed to be modeled as a uniform motion blur. Then, the parameters of the uniform motion blur, the length and angle, are estimated with an optimization technique. Though these approaches estimate an accurate PSF, they

are not applicable to the PSF which cannot be regarded as a parametric form. In many real applications, the camera tends to move in a nonlinear direction with acceleration. Therefore, the parametric estimation of the PSF sometimes yields unsatisfactory result, so that the deblurred image tends to have restoration artifacts. In this case, the parametric PSF estimation needs to be revised to estimate a more accurate PSF.

Besides, when moving objects exist or the scene has depth, the PSF changes with spatial location over the image [5]. In this case, an estimation of the LSV PSF is essential to restore the image. To deal with this problem, joint optimization of the blur identification and image restoration has been considered [6]. However, the optimization approach with the linear shift invariant (LSI) model is not numerically applicable to the LSV model. Most of the current approaches with the LSV model assume that the PSF of the image has a slow varying characteristic [7, 8]. With this assumption, the locally invariant PSF is estimated, and a piecewise invariant deconvolution is applied. The conventional piecewise invariant deblurring approaches either simply divide a whole

image only into blurred and not blurred regions [7] or use a well-known image segmentation method for the object-based processing [9]. However, since a blurred region may not have a homogeneous PSF, a single PSF for the blurred region cannot accurately describe the blur of the image. Also, the conventional image segmentation methods are not efficient for image deblurring because they generally over-segment images without considering the image blur.

In this paper, we first divide an image into multiple segments where each segment can be assumed to be blurred by the LSI PSF. Then, the LSI PSF is estimated by the proposed PSF estimation algorithm. To estimate the PSF, spreading operators are employed when they increase the accuracy of the PSF. The accuracy of the PSF is assessed by a cost function, which measures both the blur strength and undesired artifacts. Finally, image deconvolution is performed for each segment by using the estimated LSI PSF. By merging all of the resultant segments, we can obtain the deblurred image.

The rest of this paper is organized as follows. We describe the proposed PSF estimation method in Section 2 and show how to measure the amount of blurs and artifacts in Section 3. The application to the shift variant model is presented in Section 4. Experimental results and conclusion are given in Section 5 and Section 6, respectively.

2. Proposed Directional Spreading of the PSF

Before introducing the proposed method, it is worth clarifying the motivation for the proposed method. In image restoration, the image degradation [10] is generally modeled as

$$g = h * f + n, \quad (1)$$

where f , g , h , and n denote the original image, the observed image, the PSF, and the observation noise, respectively. Given h , f can be reconstructed from g by using image deconvolution algorithms [10]. However, the PSF needs to be estimated since the PSF cannot be known in real motion-blurred images. In the LSI model, the PSF is assumed to be invariant for a whole image. Then, the invariant PSF of the image is estimated by conventional techniques [2, 4]. Since most of the conventional approaches rely on a parametric model of the PSF, their estimation accuracies are dependent on the reliability of the model. Especially for the case of motion blur, the uniform motion blur model is widely adopted. However, when the camera moves to an irregular direction within an exposure time, the uniform motion blur model fails to estimate an accurate PSF. As can be seen from Figure 1, the original PSF shaped as Figure 1(a) cannot be estimated by the uniform motion blur model shown in Figure 1(b). In Figure 1, + indicates a center position of the PSF and the grey value represents a magnitude of the PSF at the corresponding coefficient. The coefficient values of the PSF vary from 0 to 1, so those values are linearly mapped from 0 to 255 for the visualization. Since image deconvolution is inherently an ill-conditioned problem, the inaccurate PSF may cause serious artifacts in the resultant

image. Therefore, in this section, we present an iterative PSF estimation technique that modifies the initial PSF at each iteration.

Figure 1(c) conceptually illustrates the expected result of the proposed method. As can be seen, the directional spreading operator can be applied to update the initial PSF for improving the accuracy of the PSF. The decision rule of applying the directional spreading operator will be explained in the next section. Given a certain decision rule, it is obvious that the estimation performance depends on the design of the spreading operator.

In this paper, we use four directional filters to spread the PSF since the combination of the four directional spreading can closely approximate the other directions. Figure 2 shows an example of directional filters whose size is 5×5 . At the previous example in Figure 1, these spreading operators are applied to the initial PSF of 64×64 size for the graphical explanation. Then, let a set of spreading operators be denoted as $S = \{s_0, s_1, s_2, s_3\}$. Each operator in S represents 1D finite impulse response (FIR) filter of four directions, that is, upper, lower, left, and right. For instance, the impulse response of the left and right directional filters, s_2 and s_3 , are defined by

$$\begin{aligned} s_2 &= [a_{-N}, a_{-N+1}, \dots, a_{-1}, a_0, 0, 0, \dots, 0], \\ s_3 &= [0, 0, \dots, 0, a_0, a_1, a_2, \dots, a_N], \end{aligned} \quad (2)$$

where a_i represents the i th coefficient and a_0 is located on the center position of this filter. If one directional operator is designed, the others are directly determined by rotating and flipping the operator.

To determine the filter coefficients, a trade-off characteristic of directional spreading operator needs to be considered. If we rapidly change the PSF by using the spreading operator, we cannot estimate an exact shape of the PSF. On the other hand, if we slowly modify the PSF, a more precise shape of the PSF can be achieved at the expense of the computational complexity. In our experiment, we decide to use a truncated-Gaussian shaped 1D filter shown in Figure 3 to slowly modify the PSF. The variance of Gaussian filter is set to 9 and the truncated coefficients are normalized to make sum equal to 1. By repeatedly applying this filter to the PSF, we can represent a more general type of blur.

Then, the spread PSF \hat{h} is obtained by the convolution of the PSF h and the spreading operator as follows:

$$\hat{h}(i, j) = \sum_{k=-N}^0 s_2(k)h(i+k, j). \quad (3)$$

Note that the length of the spreading operator is $2N+1$ but the computations are necessary for half of the elements since each operator has only $N+1$ nonzero elements. Other directional spreading are defined similarly by changing the spreading operator. This directional spreading can be regarded as a 1D filtering of the 2-D PSF matrix in a certain direction. In (3), each row of the PSF matrix is filtered using s_2 . As a result, the coefficient of the PSF matrix is spread to the left direction. This 1D directional spreading is repeatedly

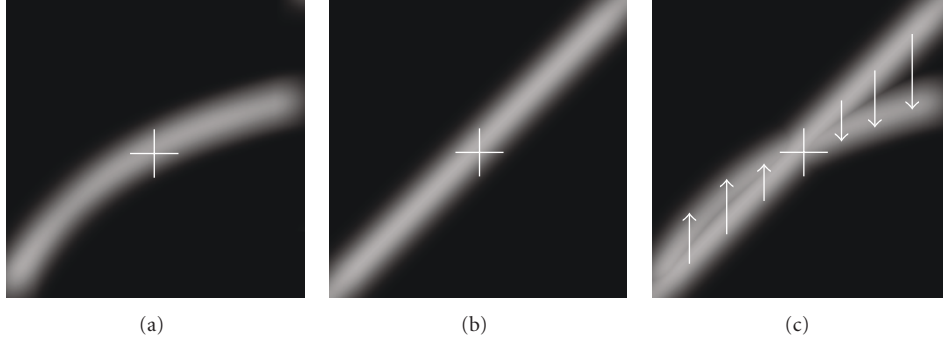


FIGURE 1: Directional spreading of the PSF. (a) Original PSF. (b) Initial PSF. (c) Directional spreading on initial PSF.

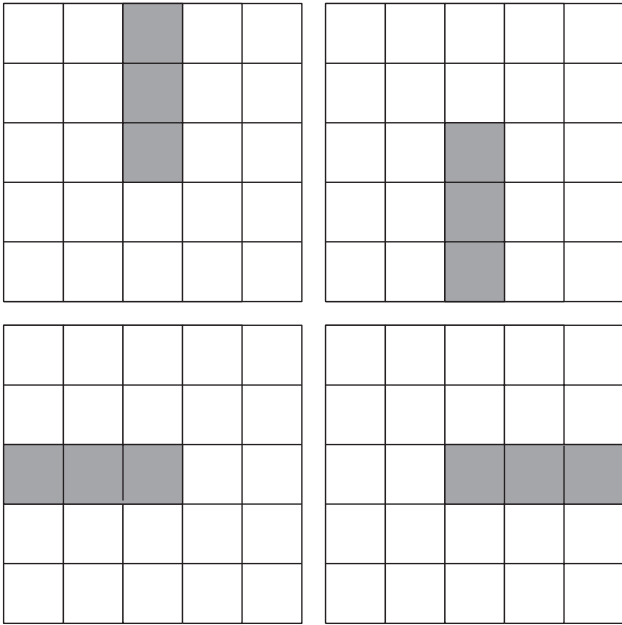


FIGURE 2: Four directional spreading operators, where the shaded position indicates nonzero element.

applied in a certain direction until the accuracy of the PSF is no more improved. Once the iteration is terminated, another spreading operator in S is adopted. The PSF update stops when all spreading operators in S are used. The remaining question is how to decide whether the PSF becomes more accurate after the directional spreading. The criterion of accuracy of the PSF is discussed in the next section.

3. Cost Function for the Accuracy of the PSF

To determine the PSF, the accuracy of the PSF needs to be measured. Since the original image is not given in the real case, quality metrics such as an improvement in the signal-to-noise ratio (ISNR) [11] are not applicable to assess the accuracy of the PSF. Therefore, we define a cost function with two assumptions. First, the accuracy of the PSF is related to the amount of blur. Indeed, the amount of blur tends to be decreased as the accuracy of the PSF increases. Second,

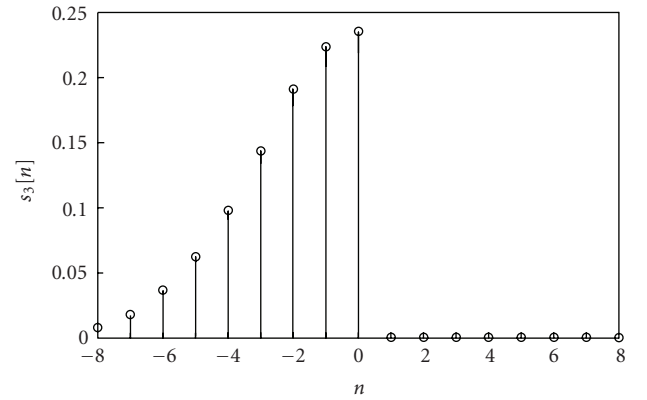


FIGURE 3: Example of directional spreading operator.

restoration artifacts of the deblurred image are dependent on the accuracy of the PSF. Due to the ill-conditioned property of the PSF, the estimation error may cause strong restoration artifacts. Therefore, the amount of the restoration artifacts is also considered in the cost function.

Since deblurring with an accurate PSF tends to reduce the blur of the image, the blur amount can be used for an accuracy measurement of the PSF. For the measurement of the blur amount, we consider the width of the edge [12]. To measure the width of an edge, or edgewidth, an edge operator is firstly applied to detect strong edges of an image. Figures 4(b) and 4(c) show the blurred image and its edgemap obtained by using the Canny edge detector [13]. Then, for each edge pixel, we find two end positions of the edge as shown in Figure 5 [12]. The distance between these two detected pixels is considered as the edgewidth. Then, the average edgewidth is used as a measure of the blur amount as follows:

$$M_B(f_0) = \frac{\sum L(f_0, E(f_0))}{\sum E(f_0)}, \quad (4)$$

where $M_B(f_0)$, $E(f_0)$, and $L(f_0, E(f_0))$ denote the blur amount, the binary edgemap, and the edgewidth image of the observed image f_0 , respectively. In $L(f_0, E(f_0))$, every edge pixel in $E(f_0)$ has the corresponding edgewidth value and

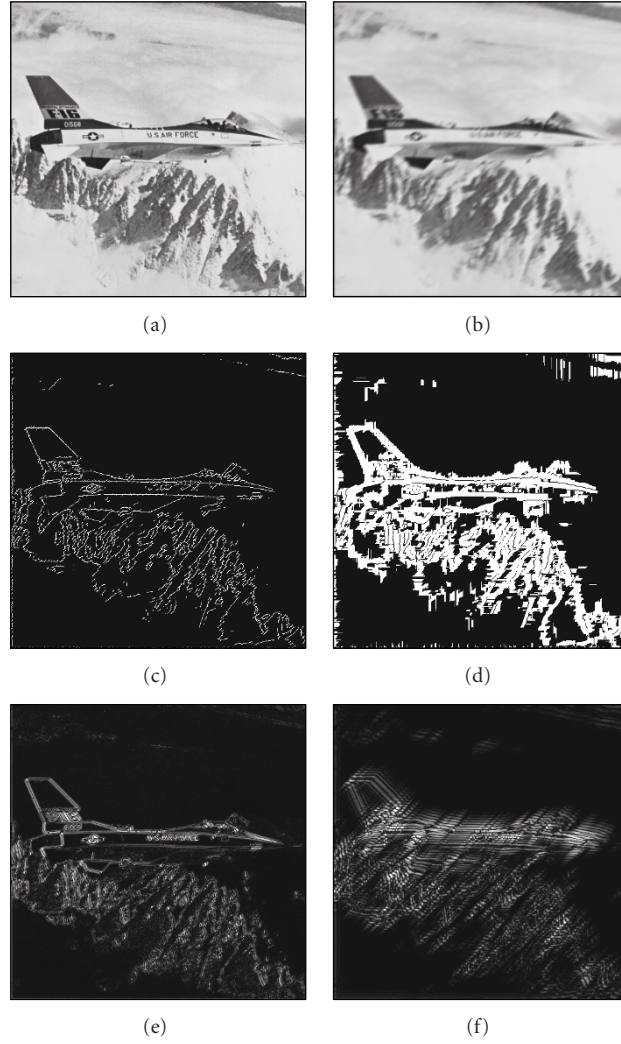


FIGURE 4: Edgewidth mask construction of observed image. (a) Original image. (b) Blurred image. (c) Edgemap of observed image. (d) Edgewidth mask. (e) Difference image between Figures 4(a) and 4(b). (f) Difference image between Figure 4(b) and the deblurred image with an inaccurate PSF.

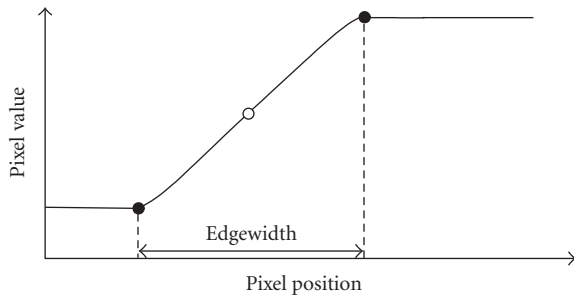


FIGURE 5: Definition of edgewidth, where a white circle represents an edge position and black circles denote end positions of the edge.

nonedge pixels have zero value. Then, the blur amount of the estimated image $M_B(\hat{f})$ is measured for each iteration as

$$M_B(\hat{f}) = \frac{\sum L(\hat{f}, E(f_0))}{\sum E(f_0)}. \quad (5)$$

Note that the edge operator is applied once to the observed image, and the blur amount is measured at each iteration with the edgemap of the observed image.

In general, an accurate PSF should not cause restoration artifacts such as ghost artifacts. Therefore, we also include restoration artifacts in the cost function. Based on the fact that the PSF has lowpass characteristics in the frequency domain, only the high-frequency region of the original image is damaged. Therefore, most changes occurred by deblurring need to be appeared in the high-frequency region that can be represented by the edges and their spread. However, if the PSF is inaccurate, deblurring may change the low-frequency regions that need to be preserved. Based on this assumption, we define a binary edgewidth mask, B_{EW} , to quantify the restoration artifacts:

$$B_{EW}(x, y) = \begin{cases} 1, & \text{if } (x, y) \in E_{sp}, \\ 0, & \text{otherwise,} \end{cases} \quad (6)$$

where E_{sp} denotes the region of edges and their spread. Specifically, if a pixel belongs to an edge or its distance from the nearest edge pixel is less than the edgewidth of the corresponding edge pixel, a pixel is included in E_{sp} . Then, the amount of change occurred outside of the edgewidth mask is used for a measurement of restoration artifact as follows:

$$M_A(\hat{f}) = \sqrt{\frac{\sum (B_{EW}^c \cdot |\hat{f} - f_o|^2)}{\sum B_{EW}^c}}, \quad (7)$$

where $M_A(\hat{f})$ denotes the amount of the restoration artifacts of the restored image, and $(^c)$ represents a bitwise complement operator.

Figures 4(e) and 4(f) exemplify the validity of the measurement for restoration artifacts. As can be seen, the change of the original image by blur largely appears in the high-frequency region. Note that the change appeared in Figure 4(e) can be covered by the edgewidth mask shown in Figure 4(d). However, the change by deblur using an inaccurate PSF cannot be covered by the edgewidth mask. Figure 4(f) represents the difference image between Figure 4(b) and the deblurred image obtained by using an inaccurate parametric PSF estimated by [7]. Due to the inaccuracy of the PSF, many changes occur outside of the edgewidth mask. Therefore, the amount of these changes can be used as the measurement of restoration artifacts.

The cost function, $C(\hat{f})$, including the amount of both blur and the artifacts is defined as

$$C(\hat{f}) = M_B(\hat{f}) + \lambda M_A(\hat{f}), \quad (8)$$

where the coefficient λ controls the weight on the restoration artifacts. This λ is dependent on the accuracy of the initial PSF estimate. Obviously, an accurate PSF should reduce the amount of blur as well as the restoration artifacts. Therefore, the spread PSF is used for the next iteration only if it reduces the cost function. The global minimum of the cost function is not assured for an arbitrarily shaped PSF caused by an irregular handshake of the camera. However, it is guaranteed that the amount of blur and restoration artifacts is reduced. Therefore, the proposed cost function can be used to increase the accuracy of the PSF when the initial PSF is not accurate.

4. Overall PSF Estimation Algorithm for the LSI Blur

In Sections 2 and 3, the directional spreading operator and the accuracy measurement method of the PSF have been presented. Now, the overall procedure of the proposed PSF estimation method needs to be considered. Figure 6 illustrates the process of the proposed PSF estimation method consisting of five steps: the initialization of the image and the PSF, image deconvolution with the previous PSF,

the modification of the PSF using a spreading operator, image deconvolution with the updated PSF, and final image deconvolution with the finally estimated PSF. For the initialization of the PSF, we adopt the uniform motion blur model [3]. Then, the directional spreading operators are used to update the PSF. By comparing the two reconstructed images, obtained by image deconvolution with different PSFs, we can determine a more accurate PSF with consideration of the cost function. Next, we present a detailed description of each step.

For the proposed PSF estimation algorithm, we assume that the PSF satisfies the nonnegativity and the energy conservation conditions defined as

$$h(x, y) \geq 0, \quad (9)$$

$$\sum_{(x,y) \in S_h} h(x, y) = 1, \quad (10)$$

where x and y are image coordinates, and S_h denotes the PSF support. The PSF support is the range that the effect of blur remains, and its size is dependent on the strength of the blur. Except for the above conditions, we do not make any assumption on the PSF to deal with a general type of motion blur.

In the initialization step of Figure 6, we assume that the PSF of the observed image f_0 can be represented by the uniform motion blur model [3] defined by

$$h_0(x, y; L, \theta) = \begin{cases} \frac{1}{C} & \text{if } \sqrt{x^2 + y^2} \leq \frac{L}{2}, \frac{y}{x} = \tan \theta, \\ 0 & \text{otherwise} \end{cases} \quad (11)$$

where x and y are PSF coordinates, L represents the length of the motion, and θ denotes the angle between the motion and the horizontal axis. The coefficient C is chosen in such a way that the condition in (10) is satisfied. Note that only two parameters, L and θ , are required to obtain the PSF. Therefore, the PSF estimation problem is reduced to the parameter estimation problem. In [7], two parameters of the uniform motion blur are estimated by using the image statistics. The blur direction, θ , is firstly selected as the direction with the minimal variation of derivatives. Then, the histogram of the derivative image is exploited to estimate L . This simple PSF estimation works only when the camera or the object moves in a linear direction with a constant speed. Therefore, we use the PSF obtained by [7] as an initial estimate. Then, the initial PSF is updated to express a more general blur of the image.

In Step 1 of Figure 6, we first perform image deconvolution to reconstruct the blurred image with the PSF which was estimated in the previous stage. Among many image deconvolution algorithms, the accelerated Richardson-Lucy (RL) deconvolution is adopted because of its reliable performance

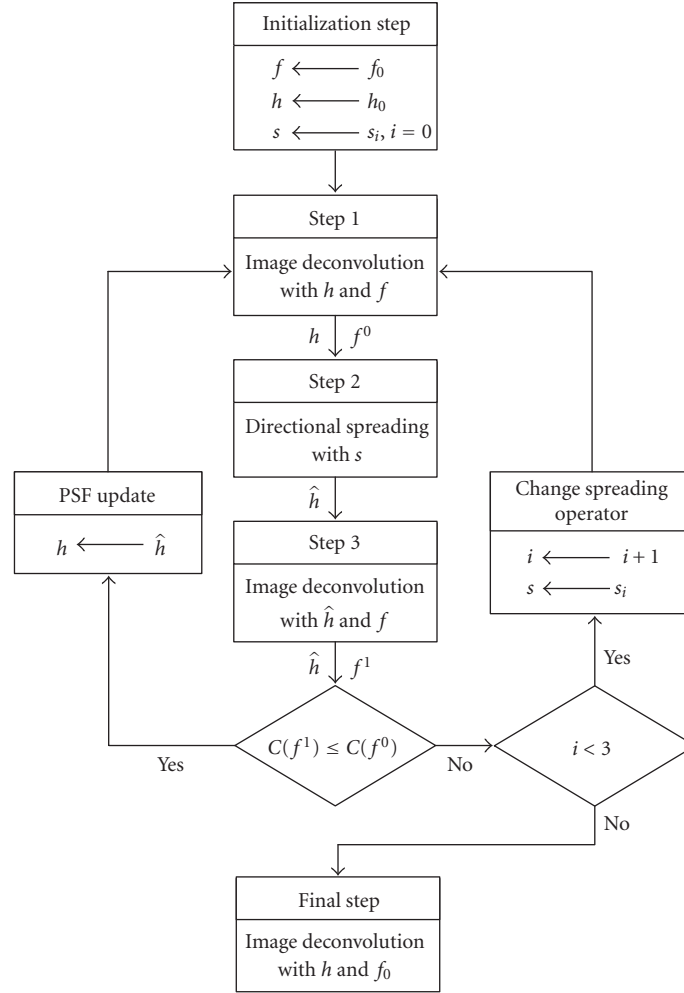


FIGURE 6: Proposed iterative PSF estimation process.

[14]. In the RL algorithm, the image f^0 is obtained by the following procedure:

(1) $k = 0$.

(2) $f_{k+1} = f_k \left(h * \frac{f_0}{h \otimes f_k} \right)$.

(3) If k reaches a predetermined iteration number,

$$f^0 = f_k.$$

Otherwise,

$$k = k + 1, \quad \text{go to (2).}$$

(12)

Then, the directional spreading operator is applied to update the PSF in Step 2. In Step 3, the image f^1 is similarly reconstructed using the RL deconvolution with the observed image and the updated spread PSF. Then, the two obtained images, f^0 and f^1 , which are restored by the previously determined PSF and the updated spread PSF, are compared by using the cost function to select a more accurate PSF.

If the spread PSF \hat{h} produces a smaller cost function value, the spread PSF is used at the next iteration. Otherwise, the spreading operator is changed to the other operator in the set S . Since this directional spreading is adopted only if it reduces the cost function, the order of the operators is not important. Once all of the spreading operators are tested, it is not necessary to repeat the overall steps. The final image is reconstructed using the RL deconvolution with the finally estimated PSF.

In addition, the spreading operator can be applied locally for increasing the accuracy of the PSF. In this case, the upper and lower direction operators, s_0 and s_1 , are examined prior to s_2 and s_3 . For each column of the PSF matrix, the spreading is applied independently, and the spread PSF is adopted only if the spreading reduces the cost function. The upward and downward spreading is performed until the cost function is not decreased. After finishing directional spreading on columns, s_2 and s_3 are similarly applied to each row of the PSF matrix. By applying this local spreading, we can estimate a more general shape of the PSF. In order to reduce the computational overhead, the local spreading is applied based on the previous spread direction. For instance, once s_0 is

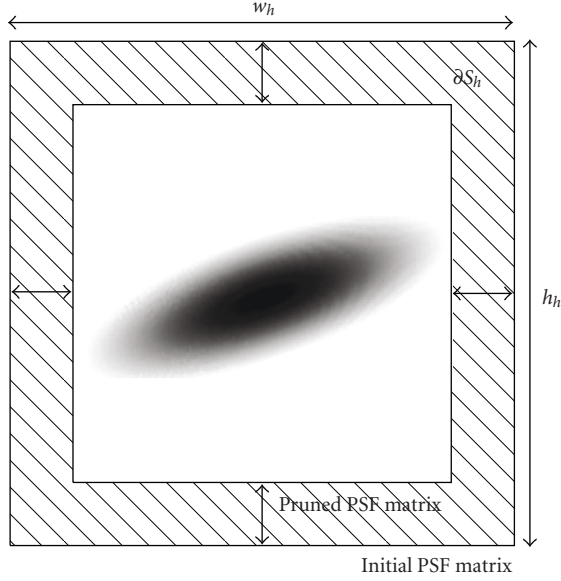


FIGURE 7: Pruning method for PSF support.

selected in a certain column, the spreading to the opposite direction, s_1 , is not performed. In other words, only one directional spreading is applied to each column. Similarly, each row is spread to the only one direction.

Also, the support of the PSF needs to be identified. A large rectangular support is assumed at the first iteration since the support of the PSF is not known in advance. Then, to decrease the computational complexity, a prune method is applied at each iteration for reducing PSF support [6]. We prune the PSF support while preserving the rectangular shape of PSF. As shown in Figure 7, the coefficients of the PSF which are located at the boundary of the rectangular support are pruned if they satisfy

$$h(x, y) \leq T, \quad (x, y) \in \partial S_h, \quad (13)$$

where T is a positive threshold and ∂S_h represents the boundary region of the PSF support. Similar to [6], the threshold T is defined as

$$T = \min\left(\frac{1}{\max(w_h, h_h)}, 0.01\right), \quad (14)$$

where w_h and h_h represent the width and height of the PSF support, respectively. Since the prune method slightly reduces the energy of the PSF, normalization is followed in order to satisfy (10).

5. Generalization to Shift Variant Blur Reduction

In the above sections, the LSI PSF estimation algorithm has been proposed. However, when the scene has depth or the relative motion is not parallel to the image plane, the LSI model is not suitable for image blur. In order to generalize the proposed algorithm, the LSV model needs to be considered. Even though the LSV PSF is given, however, deconvolution is

not directly applicable for the LSV model. Image restoration based on projection onto the convex sets (POCS) can be regarded as an alternative solution [15]. However, the LSV PSF estimation itself is indeed a difficult problem, and the POCS-based restoration is computationally complex.

Recently, the piecewise shift invariant model has been applied to the LSV image restoration [7]. The image is firstly segmented into the blurred and unblurred regions, and the RL algorithm is performed only to the blurred region by using the estimated PSF. However, this technique is applicable to the image of a single blurred object and unblurred background. In order to apply the proposed LSI deblurring technique to more general LSV image deblurring problem, we develop a piecewise shift invariant deblurring algorithm as shown in Figure 8. In our method, image segmentation method is employed to divide the image into different regions that can be considered as the LSI model. To segment the image, the amount of blur is calculated by the no-reference blur metric [12]. Since motion blur spreads the edges of the image, the length of the spread edge is relatively proportional to the amount of blur. After applying the edge operator to the blurred image, the length of spread edge is measured at every edge pixel. Pixels belonging to the edges and their spread, that is, the edgewidth mask in Section 3, are considered to be blurred pixels. Then, K -median clustering [16] with the proposed distance metric is applied to divide the blurred pixels into different regions. Within the blurred pixels, three distances including the distance of blur amount D_b , the distance of pixel value D_p , and the distance of pixel position D_d are defined to measure the similarity between two pixels, \mathbf{x}_1 and \mathbf{x}_2 , as follows:

$$\begin{aligned} D_b(\mathbf{x}_1, \mathbf{x}_2) &= |B(\mathbf{x}_1) - B(\mathbf{x}_2)|, \\ D_p(\mathbf{x}_1, \mathbf{x}_2) &= |I(\mathbf{x}_1) - I(\mathbf{x}_2)|, \\ D_d(\mathbf{x}_1, \mathbf{x}_2) &= \|\mathbf{x}_1 - \mathbf{x}_2\|_2, \end{aligned} \quad (15)$$

where B , I , and $\|\cdot\|_2$ represent the estimated blur amount, the pixel value, and the L-2 norm, respectively. Note that the blur amount of each pixel represents the edgewidth [12] as explained in the Section 3.

A scaled distance, $D_s(\mathbf{x}_1, \mathbf{x}_2)$, used for K -median clustering, is defined as a weighted sum of the three distances:

$$D_s(\mathbf{x}_1, \mathbf{x}_2) = \alpha_1 D_b(\mathbf{x}_1, \mathbf{x}_2) + \alpha_2 D_p(\mathbf{x}_1, \mathbf{x}_2) + \alpha_3 D_d(\mathbf{x}_1, \mathbf{x}_2). \quad (16)$$

After selecting the initial seeds from the blurred region, the center of each segment is iteratively modified until the cluster center is unchanged. Since D_s consists of the blur amount and the piecewise smoothness of the segment, a continuous segment with a similar blur amount can be obtained. Given the segmentation results, each segment is restored by the proposed PSF estimation method and the accelerated RL algorithm. Finally, the restoration results of all segments are merged to reconstruct the entire deblurred image.

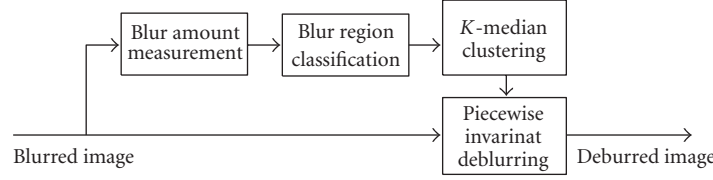


FIGURE 8: Shift variant deblurring process.

6. Experimental Results

6.1. LSI PSF Estimation Accuracy. In all of the experiments of the proposed PSF estimation, we locally spread the PSF using the four directional spreading operators defined in Section 2. In order to evaluate the performance of the proposed LSI PSF estimation, the test images, *Lena*, *Airplane*, *Barbara*, and *Peppers*, were degraded by applying the sample PSFs shown in Figure 9. Each sample PSF, h_s , was obtained by combining the uniform motion blur and the random blur as follows:

$$h_s = h_0 * h_r, \quad (17)$$

where h_0 represents the uniform motion blur defined in (11). In order to introduce a randomness of the PSF, the random blur, h_r , is combined to h_0 . Here, h_r is in a form of $N \times N$ matrix whose coefficients are randomly chosen within a range of $[0, 1]$ while satisfying (10).

Then, the degraded images are used as initial estimates of iterative PSF estimation process. For the initialization of the PSF, the length and the direction of the linear motion blur are estimated from the blurred image [7]. Figure 10 shows PSF estimation results on *Airplane* image blurred by the PSF in Figure 9(a). As can be seen from Figures 10(b), 10(c), and 10(d), the shape and the size of the PSF are efficiently estimated.

To evaluate quantitatively the performance of the proposed PSF estimation method, the quality of deblurred images of the proposed method and the conventional method is compared. Since we have original images, the ISNR [11] can be used for the quantitative measurement of the quality of the deblurred image which is defined as

$$\text{ISNR} = 10 \log \left\{ \frac{\sum_{(x,y) \in S_f} [f(x,y) - g(x,y)]^2}{\sum_{(x,y) \in S_f} [f(x,y) - \hat{f}(x,y)]^2} \right\}, \quad (18)$$

where f , g , \hat{f} , and S_f denote the original image, the blurred image, the deblurred image, and the image support, respectively. Since the ISNR increases as the quality improves, the best deblurred image is the one that has the highest ISNR.

Table 1 shows the ISNR comparison results. All of the deblurred results were obtained by 10 iterations of the accelerated RL algorithm. Since the proposed algorithm estimates the PSF from the image itself, the ISNR results were dependent on the image features. However, the results showed that the overall ISNRs of the proposed method approached those of the ideal case where the original PSF was used. From these ISNR results, we can conclude that

the proposed algorithm can estimate the PSF with a high accuracy.

In Figure 11, the normalized cost function obtained by using Figure 9(a) and *Airplane* image is illustrated, where λ is chosen as 0.5. As explained in Section 4, if a certain directional spreading reduces the cost function, the test of that direction is repeated. Otherwise, the remaining directions are tested. The proposed algorithm terminates when all the spreading operators are used. Here, the final PSF shown in Figure 10(c) was achieved after 40 updates of the PSF. Then, the accelerated RL deconvolution is applied with the estimated PSF. The original and its corresponding blurred images are given in Figures 4(a) and 4(b), and the restoration result in Figure 12 shows that the proposed method effectively restores the image without excessive restoration artifacts.

Next, we examined the performance of the proposed LSI image restoration algorithm on a real-blurred image. The test image shown in Figure 13(a) was taken with a high-end DSLR with enough exposure time for capturing the image without excessive noise. Since the image was captured with the global horizontal motion of the camera, the blur in Figure 13(a) was assumed shift invariant. The restoration result shown in Figure 13(b) demonstrates that the proposed algorithm is applicable to the real-blurred image when the PSF can be considered as the LSI.

6.2. Shift Variant Blur Reduction. In order to apply the LSI image restoration algorithm to the shift variant blur, we first experimentally generated a blurred image by applying the LSV PSF. The original image shown in Figure 14(a) contains two objects. Figure 14(b) shows a blurred image whose objects were blurred by different PSFs. As can be seen from the segmentation result in Figure 14(c), the two objects were successfully divided. In this experiment, we explicitly set the number of the segment, K , to 2. The weighting coefficients of the K -median clustering need to be carefully selected since a segmentation result is dependent on these parameters. Since we intended to divide an image into multiple regions with different blurs, we gave more weight on α_1 which measures the amount of blur. Throughout the experiment, we empirically chose α_1 , α_2 , and α_3 as 3, 2, and 1, respectively. Morphological erosion and dilation operators with a 3 by 3 rectangular structural element [17] are used for the smooth segmentation as a postfiltering. In our simulations, five iterations of dilation followed by erosion are performed to connect segments. Since conventional piecewise LSI deblurring [7] only divides the image into blurred

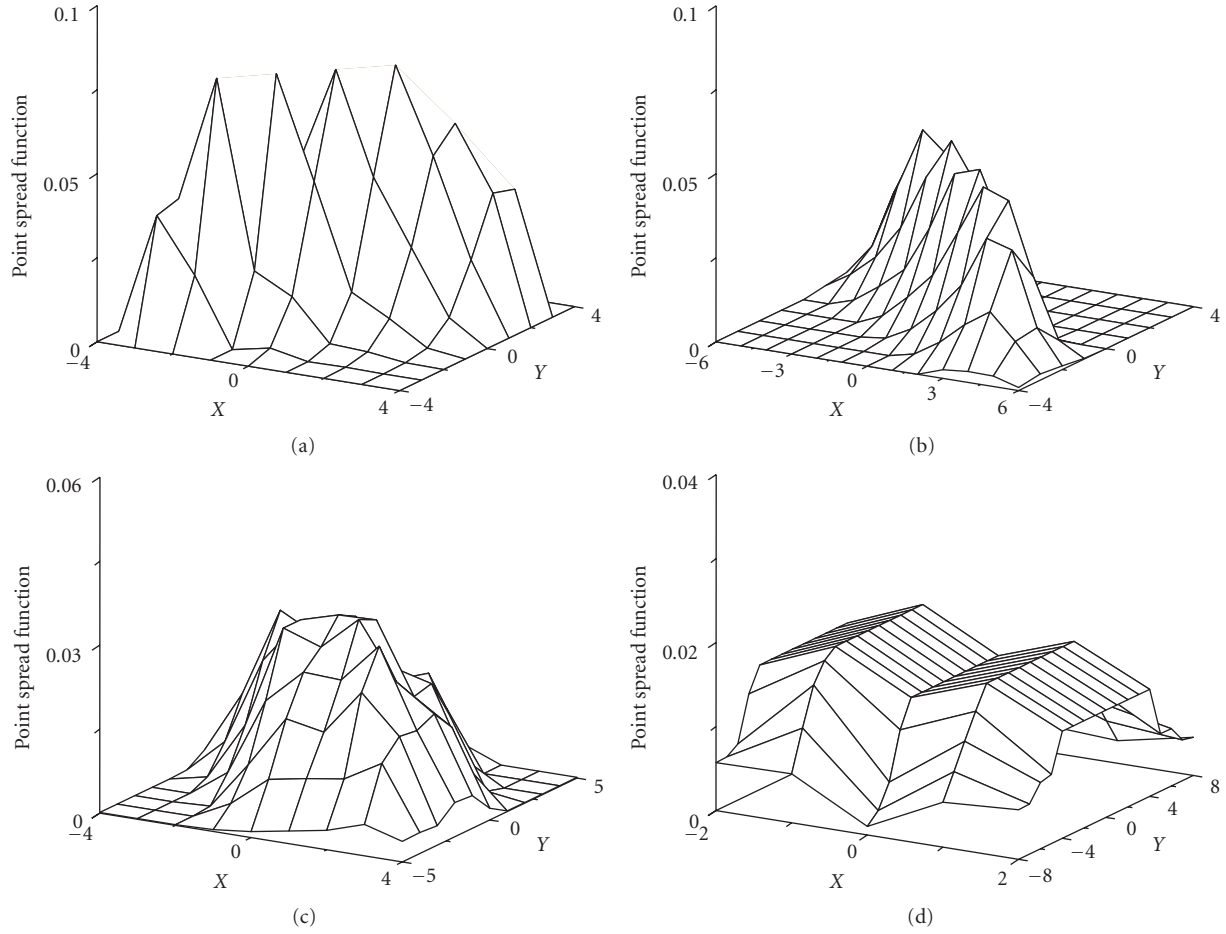


FIGURE 9: Four sample PSFs with the following parameters. (a) $L = 9$, $\theta = 135^\circ$, and $N = 3$. (b) $L = 11$, $\theta = 30^\circ$, and $N = 3$. (c) $L = 7$, $\theta = 60^\circ$, and $N = 5$. (d) $L = 13$, $\theta = 90^\circ$, and $N = 5$.

TABLE 1: ISNR(dB) comparison of deblurred results.

PSF		Image			
Original	Estimated	<i>Lena</i>	<i>Airplane</i>	<i>Barbara</i>	<i>Peppers</i>
PSF in Figure 9(a)	by [7]	1.21	0.55	1.65	1.32
	by the proposed method	3.19	2.16	2.72	3.11
	PSF in Figure 9(a)	3.57	2.82	3.05	4.88
PSF in Figure 9(b)	by [7]	1.89	2.93	3.27	3.18
	by the proposed method	3.36	3.28	3.71	4.55
	PSF in Figure 9(b)	4.19	3.62	4.12	5.02
PSF in Figure 9(c)	by [7]	0.37	0.72	0.58	0.42
	by the proposed method	2.45	3.00	2.83	2.94
	PSF in Figure 9(c)	2.79	3.29	3.01	4.12
PSF in Figure 9(d)	by [7]	0.27	0.61	0.83	1.35
	by the proposed method	1.89	2.52	1.40	2.79
	PSF in Figure 9(d)	2.35	2.69	2.14	3.36

and nonblurred regions, the quality of the deblurred image shown in Figure 14(e) is not satisfactory. The proposed segmentation-based piecewise invariant approach visually produces a better result as shown in Figure 14(f). Since the original image is given in this simulation, the ISNR can

be used to measure the quantitative performance of the results. By the comparison of ISNRs from the conventional method and the proposed method which are -1.14 and 2.03 , respectively, we see that the proposed method performs better than the conventional method.

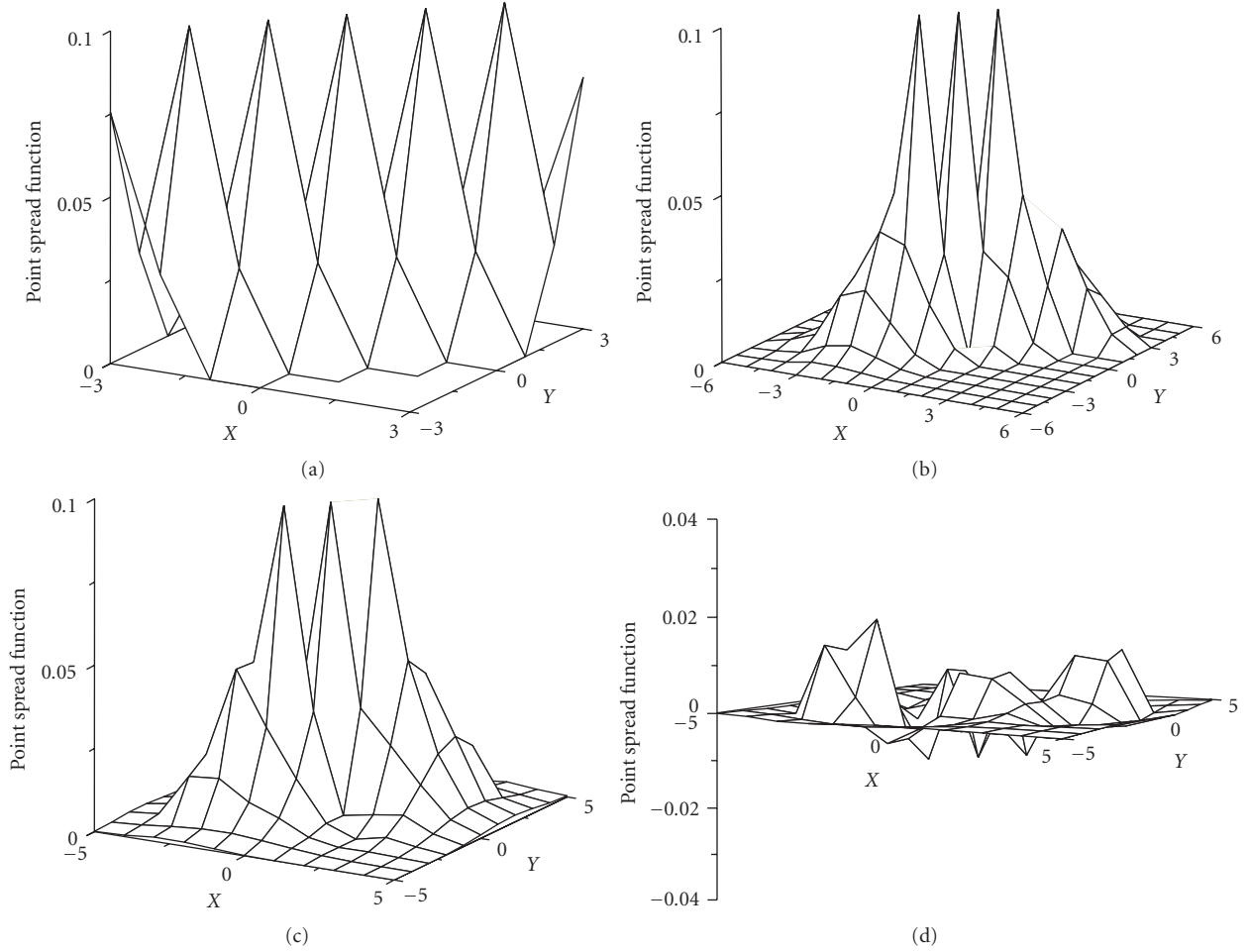


FIGURE 10: PSF estimation results using *Airplane* image and the sample PSF in Figure 9(a). (a) Initial PSF estimated by [7]. (b) Estimated PSF after 20 updates. (c) Estimated PSF after 40 updates. (d) Estimation error between Figures 9(a) and 10(c).

TABLE 2: Quantitative evaluation of deblurred results in real blurred images.

Image	Algorithm		PMOS
<i>Miniature</i>	Proposed	[7]'s	77.01
		$K = 5$	78.37
		$K = 10$	78.31
		$K = 20$	82.10
		$K = 30$	82.22
	<i>Doll</i>	Proposed	[7]'s
$K = 5$			78.42
$K = 10$			78.88
$K = 20$			79.87
$K = 30$			80.59

For the sake of implementation on image deconvolution, a rectangular segment is preferred instead of an arbitrary shaped segment. Therefore, we construct a rectangular block of minimum size for each segment. For each pixel of the segment, the minimum and the maximum pixel coordinates of the horizontal axis and the vertical axis are used to obtain the rectangular block as shown in Figure 14(d). Then, the

proposed LSI restoration is applied to each block. After LSI restoration, the actual segment region inside the block is replaced by the region of the deblurred block. Since the segment region covers most of the rectangular block, the performance is not severely compromised by introducing this simplified implementation. Finally, we obtain the restored image by merging the results of all segments. By comparing

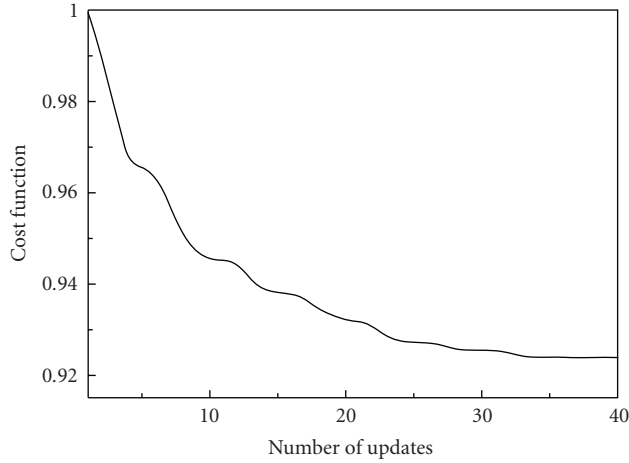


FIGURE 11: Cost function result on *Airplane* image blurred by the PSF in Figure 10(a).

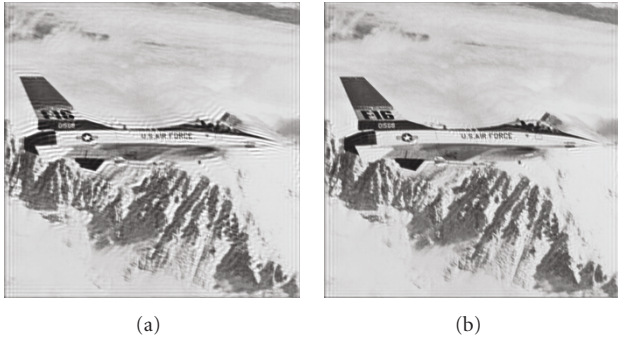


FIGURE 12: Restoration results of numerically blurred image where the PSF is estimated after 40 updates. (a) Restored image by using the conventional algorithm [7]. (b) Restored image by using the proposed.

the magnified regions of restoration results in Figures 14(g)–14(l), we can see that the proposed method outperforms the conventional method.

Next, we applied the proposed algorithm to the real blurred images also captured with a high-end DSLR. The *Miniature* image shown in Figure 15(a) was taken under 150 lux with shutter speed of 1/20 (sec) and blurred by a camera shake during the exposure time. In this high-resolution image whose spatial resolution is 1280 by 1024, the PSF of the whole image cannot be assumed to be shift invariant. Since the number of segments is not known in advance, a relatively large number should be used. We set K as 20 in this experiment. Other experimental parameters α_1 , α_2 , and α_3 are set as 3, 2, and 1, respectively. Figure 15(b) shows the segmentation result of the proposed method. In this figure, different luminance indicates a different segment. Since smooth regions are not affected by blur, those regions whose luminance is zero are not included in the segmentation. Each segment is deblurred by the aforementioned technique, and final result is compared with the result of the conventional piecewise shift-invariant approach [7]. From the magnified

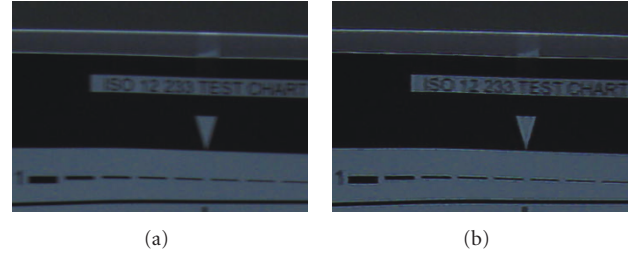


FIGURE 13: Restoration results of real-blurred image. (a) Test image. (b) Restoration result of the proposed method, where the final PSF is achieved after 27 updates.

region of each result shown in Figures 15(c)–15(f), we can subjectively compare the performances of the results.

Figure 16 shows another experimental result with a different experimental condition. The *Doll* image shown in Figure 16(a) was taken under 180 lux with shutter speed of 1/20 (sec) and blurred by a horizontal motion of camera during the exposure time. In the experiment, the same experimental parameters used in Figure 15 were maintained. As can be seen in Figure 16(b), blurred regions are separated, so each segment can be deblurred by its own estimated PSF. From the magnified region of each result shown in Figures 16(c)–16(f), we can also subjectively see the superiority of the proposed method. Note that even though the image is simply blurred by a global horizontal motion of the camera, more improved quality can be achieved by the proposed PSF estimation and piecewise LSI restoration.

We also quantitatively measured the performance of the proposed algorithm for the real blurred images. Since the original image is not given in this general restoration problem, we examined a no-reference (NR) quality assessment (QA) [18] to compare the performances of the proposed and conventional algorithms. In [18], natural scene statistics are blindly measured and the quality is expressed by the predicted mean opinion scores (PMOSs), where the higher PMOS represents the better quality. The PMOS results in Table 2 demonstrate that the proposed algorithm quantitatively performs better than the conventional algorithm.

To examine the effect of the number of segment, the results with various K are also given in Table 2. As can be seen, the performance is gradually improved as K increases until K reaches a sufficient number, which is 20. Note that K is dependent on the type of image blur. For Figure 16(a), which is blurred by a horizontal camera motion, a relatively low K provides comparable result with the results with high K . However, for an image blurred by a camera shake such as Figure 15(a), a high K is preferred to provide a sufficient quality of the resultant image.

7. Conclusion

In this paper, we presented an iterative PSF estimation method and its application to LSV image restoration. The PSF is modified by using a cost function which considers the blur strength and the restoration artifacts. Since the

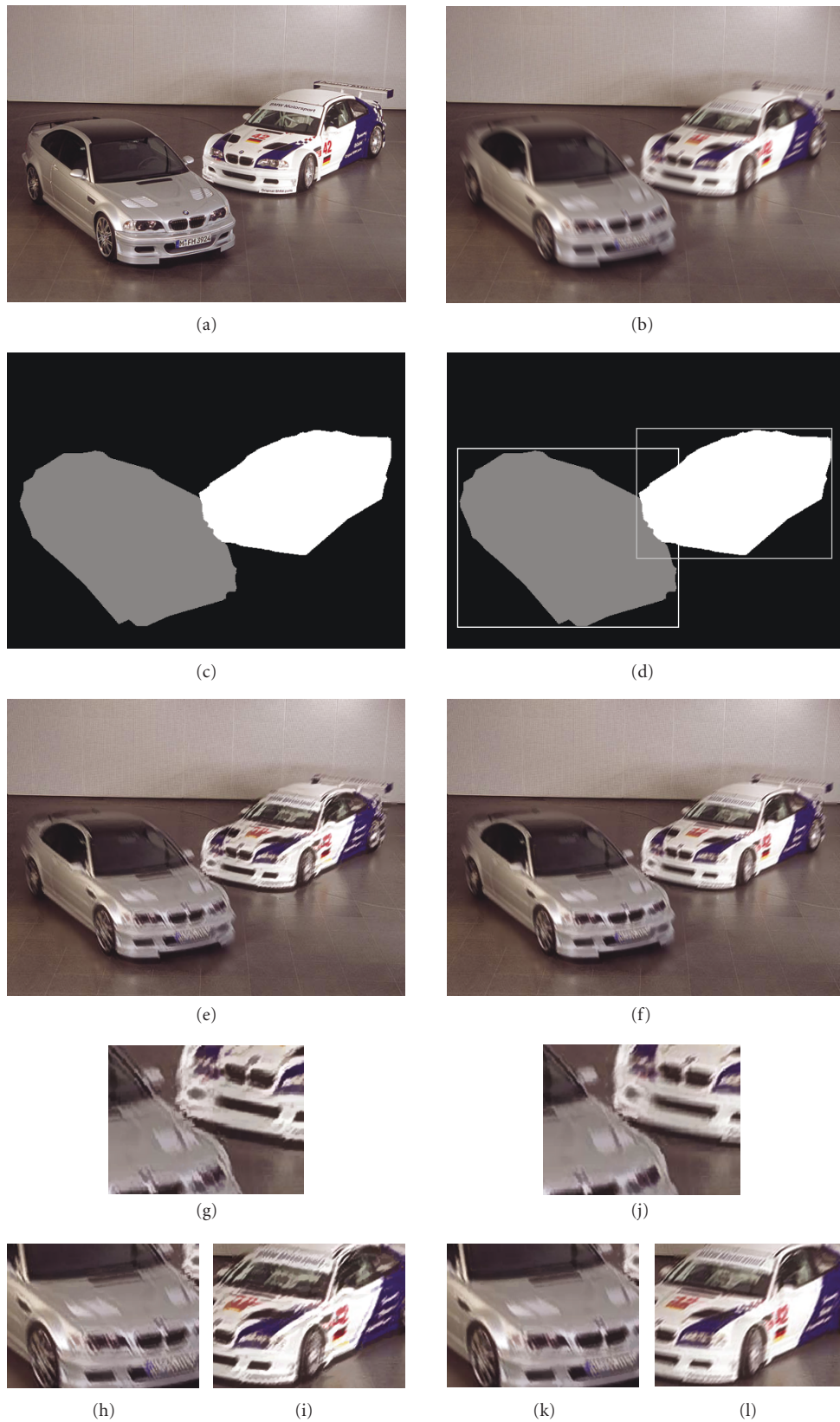


FIGURE 14: Restoration results on simulated shift variant blur images [7]. (a) Original image. (b) Blurred image. (c) Segmentation result. (d) Segmentation result with rectangular block. (e) Restoration result of [6]. (f) Restoration results of the proposed method. (g)–(i) Magnified region of Figure 14(e). (j)–(l) Magnified region of Figure 14(f).

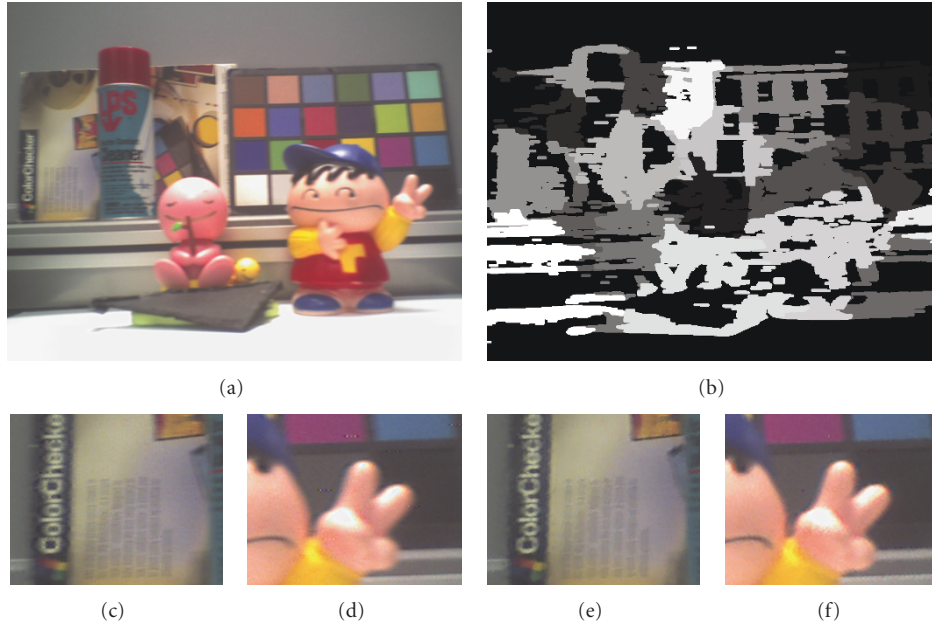


FIGURE 15: Comparison of restoration results on *Miniature* image. (a) Blurred image. (b) Segmentation result. (c)-(d) Magnified region of the deblurred image obtained by [7]. (e)-(f) Magnified region of the deblurred image obtained by the proposed algorithm.

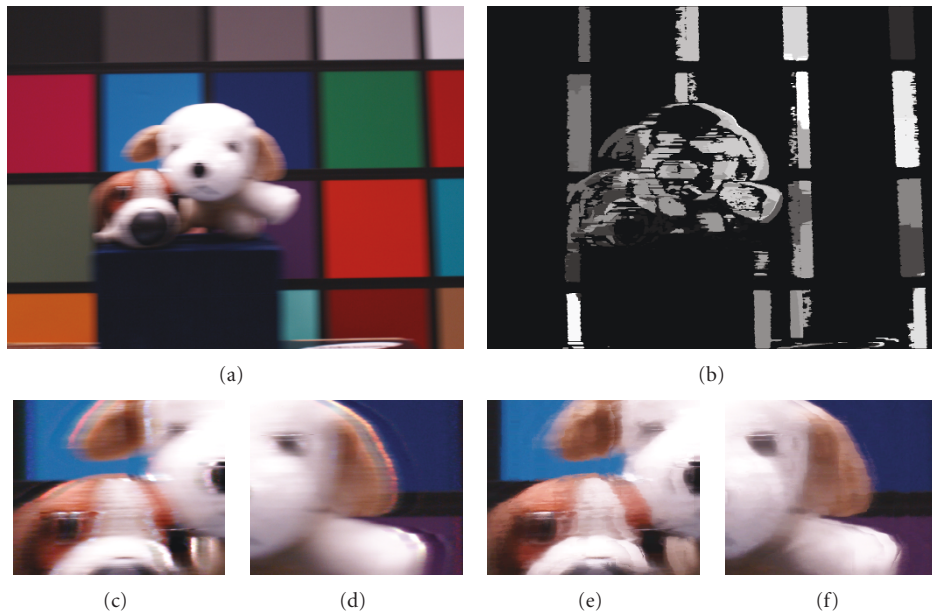


FIGURE 16: Comparison of restoration results on *Doll* image. (a) Blurred image. (b) Segmentation result. (c)-(d) Magnified region of the deblurred image obtained by [7]. (e)-(f) Magnified region of the deblurred image obtained by the proposed algorithm.

directional spreading operator is applied only when the update of the PSF reduces the cost function, the amount of blur can be decreased without excessive restoration artifacts in the restored image. Piecewise shift invariant approach with the proposed image segmentation method is applied to deal with the LSV PSF. Throughout the experiments, the proposed PSF estimation algorithm can efficiently estimate the PSF when the parametric model of the PSF is inaccurate.

The generalization of the LSI algorithm to the LSV shows relatively better performance in comparison with the conventional algorithm.

However, since the PSF update method starts from an initial estimate of the PSF, its performance tends to be affected by the accuracy of the initial guess of the PSF. To deal with the complicated PSF, which is caused by a severe handshake of the camera, more precise initial PSF estimation

methods need to be considered. In the future, we plan to extend our approach to remove motion blur of fast moving objects using video sequences.

Acknowledgment

This research was supported by Seoul Future Contents Convergence (SFCC) Cluster established by Seoul R&BD Program.

References

- [1] A. K. Katsaggelos, "Iterative image restoration algorithms," *Optical Engineering*, vol. 28, no. 7, pp. 735–748, 1989.
- [2] D. B. Gennery, "Determination of optical transfer function by inspection of frequency-domain plot," *The Optical Society of America*, vol. 63, pp. 1571–1577, 1973.
- [3] R. L. Lagendijk, J. Biemond, and D. E. Boeke, "Identification and restoration of noisy blurred images using the expectation-maximization algorithm," *IEEE Transactions on Acoustics, Speech, and Signal Processing*, vol. 38, pp. 1180–1191, 1990.
- [4] G. Pavlović and A. M. Tekalp, "Maximum likelihood parametric blur identification based on a continuous spatial domain model," *IEEE Transactions on Image Processing*, vol. 1, pp. 496–504, 1992.
- [5] D. L. Tull and A. K. Katsaggelos, "Iterative restoration of fast-moving objects in dynamic image sequences," *Optical Engineering*, vol. 35, no. 12, pp. 3460–3469, 1992.
- [6] Y.-L. You and M. Kaveh, "A regularization approach to joint blur identification and image restoration," *IEEE Transactions on Image Processing*, vol. 5, pp. 416–428, 1996.
- [7] A. Levin, "Blind motion deblurring using image statistics," in *Advances in Neural Information Processing Systems (NIPS)*, 2006.
- [8] J. Bardsley, S. Jefferies, J. Nagy, and R. Plemmons, "Blind iterative restoration of images with spatially-varying blur," *Optics Express*, vol. 14, pp. 1767–1782, 2006.
- [9] L. Bar, N. Sochen, and N. Kiryati, "Variational pairing of image segmentation and blind restoration," in *Proceedings of the 8th European Conference on Computer Vision (ECCV '04)*, Prague, Czech Republic, May 2004.
- [10] P. A. Jansson, *Deconvolution of Image and Spectra*, Academic Press, San Diego, Calif, USA, 1997.
- [11] K. L. May, T. Stathaki, and A. K. Katsaggelos, "Spatially adaptive intensity bounds for image restoration," *EURASIP Journal on Applied Signal Processing*, vol. 2003, no. 12, pp. 1167–1180, 2003.
- [12] P. Marziliano, F. Dufaux, S. Winkler, and T. Ebrahimi, "A no-reference perceptual blur metric," in *Proceedings of the International Conference on Image Processing (ICIP '02)*, vol. 3, pp. 57–60, Rochester, NY, USA, September 2002.
- [13] J. Canny, "A computational approach to edge detection," *IEEE Transactions on Pattern Analysis and Machine Intelligence*, vol. 8, pp. 679–698, 1986.
- [14] D. S. C. Biggs and M. Andrews, "Acceleration of iterative image restoration algorithms," *Applied Optics*, vol. 36, no. 8, 1997.
- [15] M. K. Ozkan, A. M. Tekalp, and M. I. Sezan, "POCS-based restoration of space-varying blurred images," *IEEE Transactions on Image Processing*, vol. 3, no. 4, pp. 450–454, 1994.
- [16] C. W. Therrien, *Decision Estimation and Classification*, IEEE Wireless Communications, John Wiley & Sons, New York, NY, USA, 1989.
- [17] R. C. Gonzalez and R. E. Woods, *Digital Image Processing*, Prentice-Hall, Upper Saddle River, NJ, USA, 2002.
- [18] H. R. Sheikh, A. C. Bovik, and L. Cormack, "No-reference quality assessment using natural scene statistics: JPEG2000," *IEEE Transactions on Image Processing*, vol. 14, no. 11, pp. 1918–1927, 2005.